# Photoinduced Charge Separation and Charge Recombination of Oligothiophene−Viologen Dyads in Polar Solvent

**Yasuyuki Araki,[†] Hongxia Luo,[†,§] Takumi Nakamura,[†] Mamoru Fujitsuka,[†,||] Osamu Ito,*[,†] Hiroki Kanato,[‡] Yoshio Aso,[‡,||] and Tetsuo Otsubo*[,‡]**

*Institute of Multidisciplinary Research for Advanced Materials, Tohoku University, Katahira, Aoba-ku, Sendai, 980-8577 Japan and Department of Applied Chemistry, Faculty of Engineering, Hiroshima University, Higashi-Hiroshima, 739-8527, Japan*

*Received: April 14, 2004; In Final Form: July 12, 2004*

Photoinduced intramolecular charge separation and charge recombination of oligothiophene−methyl viologen dyads ($T_n$−$MV^{2+}$·$2X^-$, $n = 4$ or 8, $X^- = I^-$ or $PF_6^-$), which were designed to generate positively charged radical ion pairs ($T_n^{\bullet+}$−$MV^{\bullet+}$·$2X^-$), have been investigated by the time-resolved fluorescence and transient absorption spectra in $CH_3CN$. Upon excitation of the $T_8$ moiety in $T_8$−$MV^{2+}$·$2X^-$, the radical cation pair ($T_8^{\bullet+}$−$MV^{\bullet+}$·$2X^-$) was produced via the excited singlet state of $T_8$ ($^1T_8$*), because the fluorescence lifetime of the $^1T_8$* moiety in $T_8$−$MV^{2+}$·$2X^-$ becomes short compared with pristine $^1T_8$*. The lifetimes of $T_8^{\bullet+}$−$MV^{\bullet+}$·$2X^-$ were evaluated to be 720−980 ns depending on the counteranion, $I^-$ or $PF_6^-$. On the other hand, $T_4$−$MV^{2+}$·$2X^-$ leads to lifetimes of $T_4^{\bullet+}$−$MV^{\bullet+}$·$2X^-$ of 210−240 ns, although the charge separation seems to occur via the excited triplet state of $T_4$ ($^3T_4$*), because the fluorescence quenching of the $^1T_4$* moiety in $T_4$−$MV^{2+}$·$2X^-$ was not observed. As factors to achieve these relatively long lifetimes of $T_n^{\bullet+}$−$MV^{\bullet+}$·$2X^-$, the charge recombination between of the positive charges (holes) on the $T_n$ and MV moieties and the center-to-center distance between the positive charges (holes) on the $T_n$ and MV moieties may be considered, in addition to the triplet spin character of $T_n^{\bullet+}$−$MV^{\bullet+}$·$2X^-$.

## Introduction

Photoinduced electron transfer to methyl viologen dication derivatives ($MV^{2+}$) is a key step for hydrogen gas evolution from water in the presence of appropriate sensitizers, a sacrificial donor, and a catalyst.[1−3] As photosensitizing electron donors, various organic and inorganic dyes have been applied to mixture systems with $MV^{2+}$.[1−5] Among the dyes, it has been revealed that oligothiophenes ($T_n$) act as good electron donors against an electron acceptor such as $MV^{2+}$,[6] in addition to various electron acceptors such as tetracyanoethylene, nitro compounds, and fullerenes.[6,7] In the mixture systems, the intermolecular photosensitized electron transfer usually takes place via the excited triplet states of the sensitizing dye. In such systems, both electron transfer rates and back electron transfer rates are diffusion-control limited when the processes are sufficiently exothermic, while the processes via the excited triplet states are quite $O_2$-sensitive in solution.[2,5−7]

Recently, molecular systems in which the electron donor and electron acceptor are covalently connected have been investigated.[8−11] The intramolecular through-bond charge separation process usually takes place via the excited singlet states of the sensitizing electron donor dye and/or electron acceptor dye. In general, intramolecular charge separation rates are quite faster than the intermolecular electron transfer rates via the excited triplet state.[12,13] However, the lifetimes of the charge separation states of such dyads are not long enough to mediate the electron and/or hole of the charge separation state to electron carriers and to catalysts. Recently, several molecular dyad systems with sufficiently long-lived charge separation states have been reported.[14] In the molecular design of the dyads attaining the long-lived charge separation states, the free-energy changes for the charge separation and charge recombination processes should be adjusted to be the top region and the inverted region of the Marcus parabola, respectively.[15] Dyads including a fullerene are thought to be appropriate molecules for generating a long-lived charge separation state because of the small reorganization energy of fullerenes.[16] In addition, when the excited triplet state of the component has very similar energy to the charge separation state, the radical ion pair can easily gain triplet spin character leading to further long lifetimes of the charge separation states.[17]

In the present study, we designed the dyad molecular systems with viologen dication derivatives so as to have two positive charges in the charge separation state in the dyad, in which retardation of the charge recombination process between positively charged moieties would be anticipated. As an electron donor, we employed $T_n$ ($n = 4$ or 8), showing appreciable absorption bands in the visible region to efficiently utilize solar energy. In addition, because spectroscopic properties of the radical cations of $T_n$ are well-characterized by the transient absorption,[6,7,18−21] the charge separation and charge recombination processes upon photoexcitation can be followed unequivocally. From these viewpoints, dyad molecules of $T_n$ covalently connected to the viologen moiety ($T_n$−$MV^{2+}$·$2X^-$, $n = 4$ or 8, $X^- = I^-$ or $PF_6^-$; Scheme 1) have been designed. To reveal the photoinduced charge separation processes via the excited

* Authors for correspondence. E-mail: ito@tagen.tohoku.ac.jp (O.I.); otsubo@hiroshima-u.ac.jp (T.O.).
† Tohoku University.
‡ Hiroshima University.
§ Present address: Department of Chemistry, Renmin University of China, Beijing 100872, China.
|| Present address: The Institute of Scientific and Industrial Research, Osaka University, Osaka 567-0047, Japan.

10.1021/jp048364r CCC: $27.50 
Published on Web 11/04/2004

**SCHEME 1**

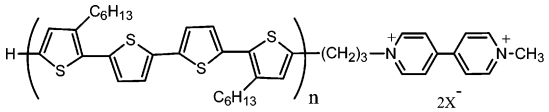


n = 1: $T_4$-$MV^{2+}$
n = 2: $T_8$-$MV^{2+}$

$X^- = PF_6^-$ or $I^-$

state of the $T_n$ moiety in $T_n-MV^{2+}\cdot 2X^-$, we employed time-resolved fluorescence measurements and transient absorption measurements in the visible and near-IR regions.

## Results and Discussion

**Synthesis.** $T_8-MV^{2+}\cdot 2X^-$ (1-[3-(3,3′,4′,3″-tetrahexyl-2,2′;5′,2″;5″,2‴;5‴,2⁗,5⁗, 2⁗;5⁗,2⁗⁗-octithiophen-5-yl)propyl]-1′-methyl-4,4′-bipyridinium salt) and $T_4-MV^{2+}\cdot 2X^-$ (1-[3-(3,3‴-dihexyl-2,2′;5′,2″;5″,2‴-quaterthiophen-5-yl)propyl]-1′- methyl-4,4′-bipyridinium salt), in which $X^- = I^-$ and $PF_6^-$, were prepared by the method described in the Experimental Section in detail. Briefly, one α-carbon of $T_8$ or $T_4$ was haloalkylated with dihalogenated propane after treatment with BuLi.[22a] Cross-coupling of 1-methyl-4,4′-bipyridinyl-1-ium iodide ($MV^+\cdot I^-$) with iodopropyl $T_8$ or iodopropyl $T_4$ yielded $T_8-MV^{2+}\cdot 2I^-$ or $T_4-MV^{2+}\cdot 2I^-$, respectively.[22b] For $X^- = PF_6^-$, the anion was exchanged using $NH_4PF_6$.

**Molecular Orbital Calculation.** Figure 1 shows the optimized structure of $T_8-MV^{2+}$ calculated by PM3 without considering counteranions.[23] The center-to-center distance ($R_{CC}$) was evaluated from the distance between the centers of the electron distribution of $T_8$ and $MV^{2+}$ to be 21.8 Å. The $T_8$ and $MV^{2+}$ moieties are in a V-shape, bending at the propane linker. The HOMO and LUMO localized on the $T_8$ and $MV^{2+}$moieties, respectively, which suggests that the hole distribution localizes in the $T_8$ moiety, while the extra electron distributes on the $MV^{2+}$ moiety, generating the charge separation state like $T_8^{\bullet+}-MV^{\bullet+}$. It is also predicted that the first electronic transition is the charge transfer transition.

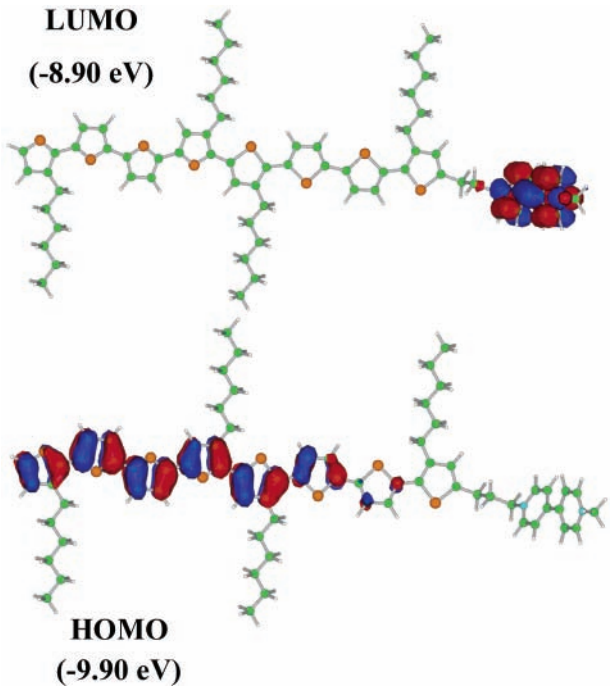


**Figure 1.** Optimized structure and the HOMO and LUMO of $T_8-MV^{2+}$.

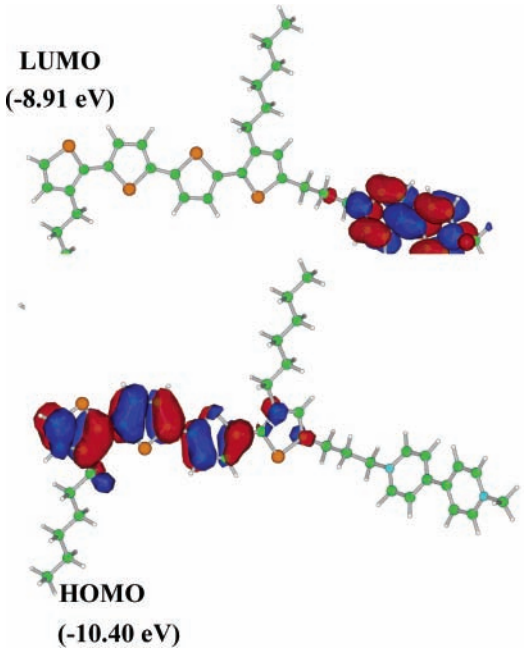


**Figure 2.** Optimized structure and the HOMO and LUMO of $T_4-MV^{2+}$.

**TABLE 1: Oxidation Potentials ($E_{ox}$'s), Reduction Potentials ($E_{red}$'s), Excited Singlet State ($E_S$), and Excited Triplet State ($E_T$) of $T_n-MV^{2+}\cdot 2X^-$ in $CH_3CN$[a]**

| dyad | X | $E_{ox}$/V | $E_{red}$/V | $E_S$/eV | $E_T$/eV |
|---|---|---|---|---|---|
| $T_8-MV^{2+}$ | $PF_6^-$ | 0.30 | −0.92 | 2.31 | 1.60 |
| $T_8-MV^{2+}$ | $I^-$ | 0.30 | −0.87 | 2.31 | 1.60 |
| $T_4-MV^{2+}$ | $PF_6^-$ | 0.50 | −0.87 | 2.70 | 1.83 |
| $T_4-MV^{2+}$ | $I^-$ | 0.50 | −0.87 | 2.70 | 1.83 |

[a] $E_{ox}$ and $E_{red}$ values are vs $Fc/Fc^+$. $E_{0-0}$ is for excited singlet state ($E_S$) and excited triplet state ($E_T$).

In the case of $T_4-MV^{2+}$ (Figure 2), the $R_{CC}$ was evaluated to be 11.3 Å. The HOMO and LUMO of $T_4-MV^{2+}$ are shown in Figure 2. The electron densities of the HOMO and LUMO localize in the $T_4$ and $MV^{2+}$ moieties, respectively, generating the charge separation state, $T_4^{\bullet+}-MV^{\bullet+}$.

**Electrochemistry.** The first oxidation potentials ($E_{ox}$'s) of $T_8-MV^{2+}\cdot 2PF_6^-$ and $T_4-MV^{2+}\cdot 2PF_6^-$ were evaluated to be 0.30 and 0.50 V versus ferrocene/ferrocenium ($Fc/Fc^+$) in $CH_3CN$, which are attributed to the oxidation of the $T_8$ and $T_4$ moieties, respectively. The $T_8$ moiety is easily oxidized compared with the $T_4$ moiety. The reduction potentials ($E_{red}$'s) of $T_8-MV^{2+}\cdot 2PF_6^-$ and $T_4-MV^{2+}\cdot 2PF_6^-$ were evaluated to be −0.92 V and −0.87 V versus $Fc/Fc^+$, respectively, which are attributed to the reduction of the $MV^{2+}$ moiety. These values are summarized in Table 1. These $E_{ox}$ values were not varied by replacing the counteranion from $2PF_6^-$ to $I^-$, while the $E_{red}$ of $T_8-MV^{2+}\cdot 2I^-$ was less negative than that of $T_8-MV^{2+}\cdot 2PF_6^-$, probably because of aggregation due to its lower solubility in $CH_3CN$ than $T_8-MV^{2+}\cdot 2PF_6^-$. The free-energy changes ($\Delta G_{RIP}$'s) of the radical ion pairs ($T_n^{\bullet+}-MV^{\bullet+}$), charge separation ($\Delta G_{CS}$), and charge recombination ($\Delta G_{CR}$) were calculated by eqs 1 and 2.[24]

$$\Delta G_{RIP} = -\Delta G_{CR} = -E_{ox} + E_{red} - \Delta G_S \quad (1)$$

$$-\Delta G_{CS} = \Delta E_{0-0} - \Delta G_{RIP} \quad (2)$$

In eqs 1 and 2, $\Delta E_{0-0}$ and $\Delta G_S$ refer to the lowest excited-state energy of $T_n$ and the solvation energy change between $T_n-MV^{2+}$ and $T_n^{\bullet+}-MV^{\bullet+}$, respectively.

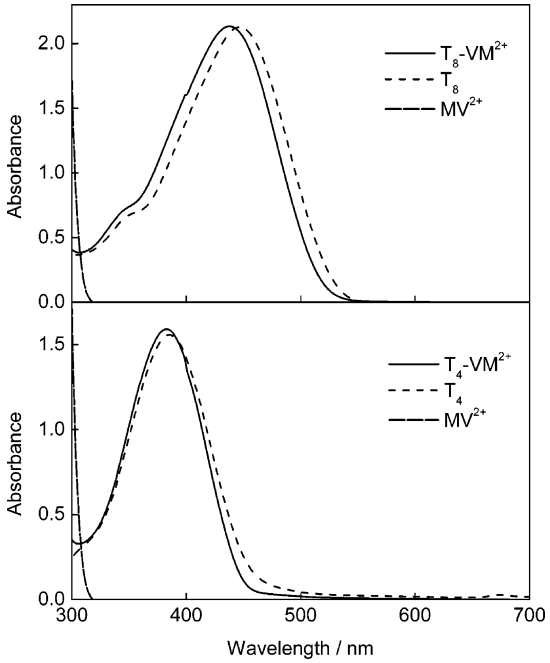


**Figure 3.** Steady-state absorption spectra of (A) $T_8-MV^{2+}\cdot 2PF_6^-$, $T_8$, and $MV^{2+}$ (0.05 mM) and (B) $T_4-MV^{2+}\cdot 2PF_6^-$, $T_4$, and $MV^{2+}$ (0.05 mM) in $CH_3CN$.

**Steady-State Absorption Spectra.** $T_8-MV^{2+}\cdot 2PF_6^-$ and $T_4-MV^{2+}\cdot 2PF_6^-$ showed absorption peaks at 437 and 382 nm (Figure 3), respectively, which are attributed to the absorption of the $T_8$ and $T_4$ moieties. The molecular extinction coefficients of these bands are similar to the corresponding $T_n$; thus, the interaction between the $T_n$ and $MV^{2+}$ moieties is weak in the ground states of $T_n-MV^{2+}\cdot 2X^-$. Slight shifts of the absorption bands were observed, which are probably caused by the substituent effect of the oligothiophenes and/or the charge transfer transition. Because the absorption band of $MV^{2+}$ appears in a shorter wavelength than 300 nm, the laser light at 355 nm predominantly excites the $T_n$ moieties of $T_n-MV^{2+}\cdot 2PF_6^-$. Absorption spectra of $T_n-MV^{2+}\cdot 2I^-$ are similar to those of $T_n-MV^{2+}\cdot 2PF_6^-$.

**Steady-State Fluorescence Spectra.** $T_8-MV^{2+}\cdot 2PF_6^-$ and $T_4-MV^{2+}\cdot 2PF_6^-$ showed the fluorescence peaks at 540 and 465 nm (Figure 4), respectively, which are attributed to the $T_8$ and $T_4$ moieties, respectively. The Stokes shifts of $T_n-MV^{2+}\cdot 2PF_6^-$ and $T_4-MV^{2+}\cdot 2PF_6^-$ are 4360 and 4670 $cm^{-1}$, respectively. Because $T_8-MV^{2+}\cdot 2PF_6^-$ and $T_4-MV^{2+}\cdot 2PF_6^-$ are insoluble in nonpolar solvents such as toluene, it is impossible to elucidate the charge separation process via the excited singlet states of the $T_n$ ($^1T_n$*) moieties from the degree of quenching of the fluorescence intensities. Fluorescence spectra of $T_n-MV^{2+}\cdot 2I^-$ are similar to those of $T_n-MV^{2+}\cdot PF_6^-$.

**Fluorescence Lifetimes.** In the inset of Figure 4, the fluorescence decays of $T_8-MV^{2+}\cdot 2PF_6^-$ and $T_4-MV^{2+}\cdot 2PF_6^-$ in $CH_3CN$ are shown. In the case of $T_8-MV^{2+}\cdot 2PF_6^-$, the fluorescence time profile was analyzed with biexponential functions giving lifetimes ($\tau_f$ values) of 20 ps (60%) and 730 ps (40%). The fluorescence of $T_8$ decayed with a single-exponential function giving $\tau_f$ of 730 ps. A further short $\tau_f$ value was evaluated for $T_8-MV^{2+}\cdot 2I^-$ as listed in Table 2. From these short fluorescence lifetimes observed for $T_8-MV^{2+}\cdot 2X^-$, it is revealed that the charge separation process takes place via the excited singlet state of the $T_n$ moiety. The rate constants ($k^S_{CS}$'s) for the charge separation process via the $^1T_n$* moieties were evaluated using eq 3.

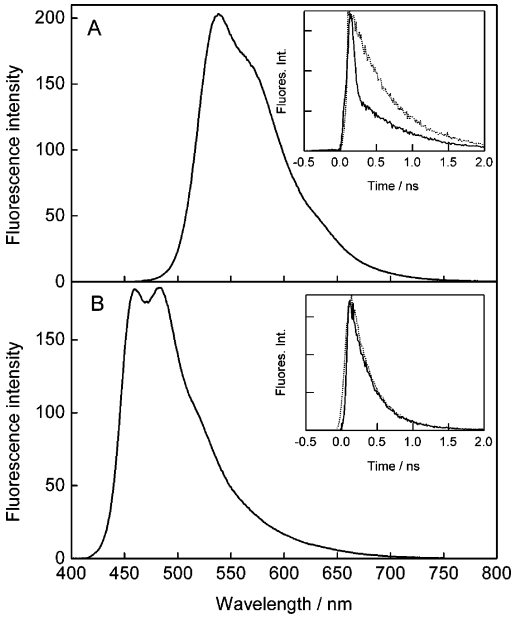


**Figure 4.** Steady-state fluorescence spectra of (A) $T_8-MV^{2+}\cdot 2PF_6^-$ (0.05 mM) and (B) $T_4-MV^{2+}\cdot 2PF_6^-$ (0.05 mM) in $CH_3CN$; $\lambda_{ex} = 383$ nm. Inset: Fluorescence decay profiles at 550 nm for $T_8-MV^{2+}\cdot 2PF_6^-$ and 480 nm for $T_4-MV^{2+}\cdot 2PF_6^-$.

**TABLE 2: Fluorescence Lifetimes ($\tau_f$'s), Rate Constants ($k^S_{CS}$'s), Quantum Yields ($\Phi^S_{CS}$'s), and Free-Energy Changes ($\Delta G_{CS}$'s) for Charge Separation of $T_n-MV^{2+}\cdot 2X^-$ in $CH_3CN$**

| dyad | $X^-$ | $\tau_f$/ps | $k^S_{CS}{}^a/s^{-1}$ | $\Phi^S_{CS}{}^b$ | $\Delta G^S_{CS}{}^c$/ eV | $\Delta G^T_{CS}{}^c$/ eV |
|---|---|---|---|---|---|---|
| $T_8-MV^{2+}$ | $PF_6^-$ | 20 (60%), 730 (40%) | $4.9 \times 10^{10}$ | 0.60 | −1.10 | −0.40 |
| $T_8-MV^{2+}$ | $I^-$ | 10 (65%), 720 (35%) | $9.9 \times 10^{10}$ | 0.65 | −1.05 | −0.36 |
| $T_4-MV^{2+}$ | $PF_6^-$ | 380 (100%) | ($k^T_{CS} > 10^8$) | | −1.34 | −0.38 |
| $T_4-MV^{2+}$ | $I^-$ | 390 (100%) | ($k^T_{CS} > 10^8$) | | −1.34 | −0.38 |

[a] For $T_8$, $(\tau_f)_{ref} = 730$ ps, and for $T_4$, $(\tau_f)_{ref} = 390$ ps. From the fast fluorescence lifetimes. [b] From the fraction of fast fluorescence decays. [c] $\Delta G_S = e^2/(4\pi\epsilon_0\epsilon_s)\,(1/2R_+(T_n) + 1/2R_+(MV) + 1/R_{cc})$; $R_+(T_n)$ and $R_+(MV)$ are radii of the ion radicals of $T_n$ (6.6 Å for $T_8$ and 6.4 Å for $T_4$) and $MV^{2+}$ (3.1 Å), respectively; $R_{CC}$ is the center-to-center distance between the two moieties (21.8 Å for $T_8-MV^{2+}$ and 11.3 Å for $T_4-MV^{2+}$); $\epsilon_s$ is the dielectric constant of solvent.

$$k^S_{CS} = (1/\tau_f)_{sample} - (1/\tau_f)_{ref} \qquad (3)$$

where $(1/\tau_f)_{sample}$ and $(1/\tau_f)_{ref}$ are reciprocals of the fluorescence lifetimes of the $^1T_n$* moiety of the dyad and of the pristine $^1T_n$*, respectively. The $k^S_{CS}$ values are summarized in Table 2. In the cases of $^1T_8$*$-MV^{2+}\cdot 2X^-$, a fast charge separation process was confirmed for both counteranions in $CH_3CN$. The $k^S_{CS}$ value for $^1T_8$*$-MV^{2+}\cdot 2I^-$ is slightly larger than $^1T_8$*$-MV^{2+}\cdot 2PF_6^-$. The quantum yields ($\Phi^S_{CS}$'s) for the charge separation process via the $^1T_8$* moiety were approximated from the fraction of the fast fluorescence decay. The remaining slow fluorescence decay part may be attributed to the intersystem crossing (ISC).

The fluorescence time profiles of the $^1T_4$* moiety of $T_4-MV^{2+}\cdot 2X^-$ were analyzed with a single-exponential function giving $\tau_f = 380$ ps, which is almost the same as that of the pristine $^1T_4$* in $CH_3CN$ (inset of Figure 4), suggesting that the charge separation process does not take place via the $^1T_4$* moiety in $T_4-MV^{2+}\cdot 2X^-$. The $^1T_4$* moiety in $T_4-MV^{2+}\cdot 2X^-$ is converted to the triplet state via ISC without the charge separation process.

**Nanosecond Transient Spectra.** The absorption spectrum of the radical cation of $T_8$ ($T_8^{\bullet+}$) observed upon addition of

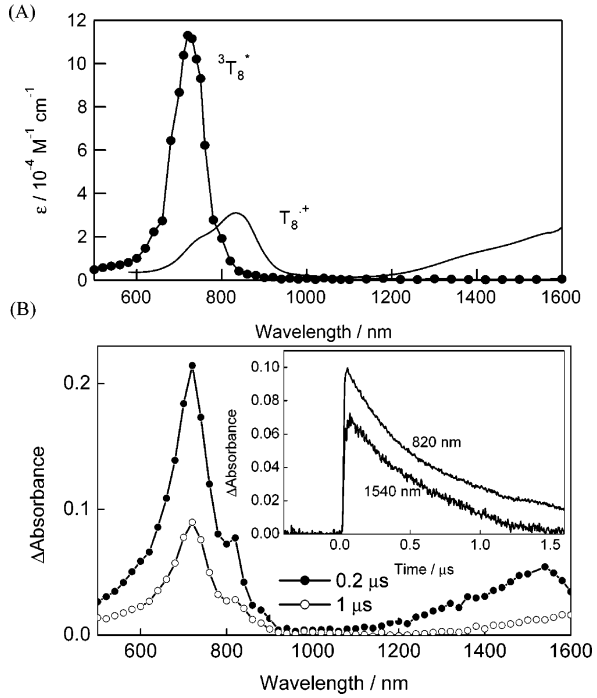


**Figure 5.** (A) Absorption spectrum of radical cation of $T_8$ (line) and transient absorption spectrum of triplet state of $T_8$ in $CH_3CN$. (B) Nanosecond transient absorption spectra of $T_8-MV^{2+}\cdot 2PF_6^-$ (0.1 mM) in Ar-saturated $CH_3CN$ after the 355-nm laser irradiation. Inset: Time profiles of absorbance at 820 and 1540 nm.

$FeCl_3$ is shown in Figure 5A, in which the molar extinction coefficients of $T_8^{\bullet+}$ were evaluated from the consumption of $T_8$. In Figure 5A, the triplet−triplet absorption spectrum of $T_8$ ($^3T_8$*) observed by nanosecond laser-light irradiation is also shown. The molar extinction coefficients of $^3T_8$* were evaluated from comparison with those of $^3C_{60}$*.[25] Nanosecond transient spectra of $T_8-MV^{2+}\cdot 2PF_6^-$ observed by the excitation of the $T_8$ moiety are shown in Figure 5B, which exhibits the appearance of the $T_8^{\bullet+}$ moiety at 1550 and 850 nm. From the molar extinction coefficients of $T_8^{\bullet+}$ ($\epsilon_{T8^{\bullet+}} = 32\,000$ and $21\,000$ $M^{-1}$ $cm^{-1}$ at 850 and 1550 nm, respectively), the concentration of the $T_8^{\bullet+}$ moiety at 0.2 $\mu$s after the nanosecond laser-light pulse was evaluated to be about $2.2 \times 10^{-6}$ M. The absorption of the $MV^{\bullet+}$ moiety, which was expected to appear in the 500−750 nm region with the main peak at 590−610 nm,[26] was not clearly observed in Figure 5B, probably because the absorption band of the $MV^{\bullet+}$ moiety may be hidden by the absorption tail of the intense absorption of $T_8^{\bullet+}$ at 850 nm and the $^3T_8$* moiety ($\epsilon_{^3T^*} = 115\,000$ $M^{-1}$ $cm^{-1}$ at 740 nm), because the molar extinction coefficient of the $MV^{\bullet+}$ moiety ($\epsilon_{MV^{\bullet+}} = 13\,700$ $M^{-1}$ $cm^{-1}$ at 600 nm)[26b] is slightly smaller than the added value of $T_8^{\bullet+}$ (4300 $M^{-1}$ $cm^{-1}$) and $^3T_8$* (10 200 $M^{-1}$ $cm^{-1}$) at 600 nm. From the short fluorescence lifetimes, it is obvious that the charge separation process takes place mainly via $^1T_8$*$-MV^{2+}\cdot 2X^-$ in $CH_3CN$. The time profile of the transient absorption band at 1500 nm gave a charge recombination rate constant ($k_{CR}$) in the region of $1.0-1.4 \times 10^5$ $s^{-1}$ (Table 3), from which the lifetimes ($\tau_{RIP}$ values) of $T_8^{\bullet+}-MV^{\bullet+}\cdot 2X^-$ were calculated to be 720−980 ns. One of the reasons for such long $\tau_{RIP}$ values can be attributed to the charge recombination between the positively charged species.

The maximal concentration of $^3T_8$*$-MV^{2+}\cdot 2X^-$ immediately after the laser pulse was $1.5 \times 10^{-6}$ M. Thus, the ratio of $T_8^{\bullet+}$:$^3T_8$* is 3:2. This ratio is in good agreement with the ratio of the quantum yields $\Phi^S_{CS}$:$\Phi^S_{ISC}$. Therefore, the route of $^3T_8$* formation is the ISC process via $^1T_8$*. As shown in Figure 6,

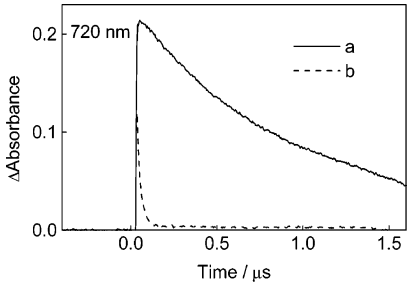


**Figure 6.** Time profiles of absorbance at 720 nm for $T_8-MV^{2+}\cdot 2PF_6^-$ (0.05 mM) (a) in Ar-saturated $CH_3CN$ and (b) in $O_2$-saturated $CH_3CN$.

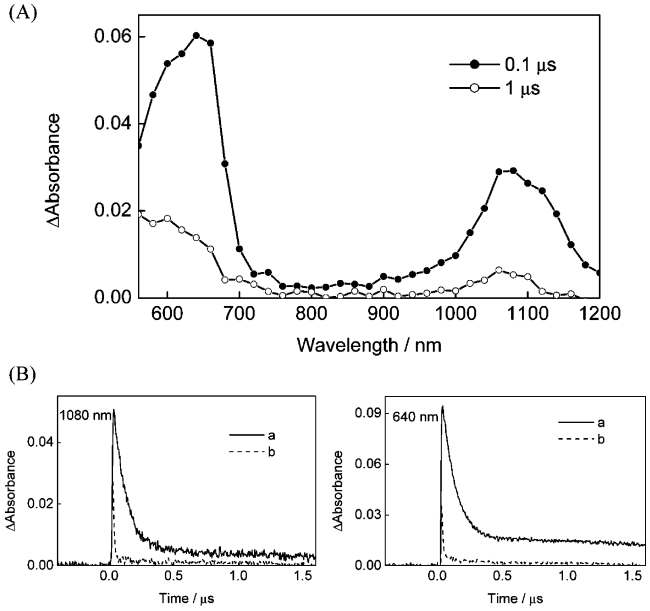


**Figure 7.** (A) Nanosecond transient absorption spectra of $T_4-MV^{2+}\cdot 2PF_6^-$ (0.1 mM) in Ar-saturated $CH_3CN$ after the 355-nm laser irradiation. (B) Time profiles of absorbance at 640 and 1080 nm (a) in Ar-saturated and (b) in $O_2$-saturated $CH_3CN$.

**TABLE 3: Rate Constants ($k_{CR}$'s) and Free-Energy Changes ($\Delta G_{CR}$'s) for Charge Recombination and Lifetimes ($\tau_{RIP}$'s) of $T_n-MV^{2+}\cdot 2X^-$ in $CH_3CN$**

| dyad | $X^-$ | $k_{CR}/s^{-1}$ | $\tau_{RIP}$/ns | $\Delta G_{CR}$/eV |
|---|---|---|---|---|
| $T_8-MV^{2+}$ | $PF_6^-$ | $1.4 \times 10^5$ | 720 | −1.24 |
| $T_8-MV^{2+}$ | $I^-$ | $1.0 \times 10^5$ | 980 | −1.19 |
| $T_4-MV^{2+}$ | $PF_6^-$ | $4.2 \times 10^6$ | 240 | −1.44 |
| $T_4-MV^{2+}$ | $I^-$ | $4.8 \times 10^6$ | 210 | −1.44 |

$^3T_8$*$-MV^{2+}\cdot 2X^-$ in Ar-saturated $CH_3CN$ decays with lifetime of 1000 ns, which is similar to that of $T_8^{\bullet+}-MV^{\bullet+}\cdot 2X^-$, although the lifetime of the pristine $^3T_8$* was reported to be 18 000 ns.[20b] This observation strongly suggests that there is rapid equilibrium between $T_8^{\bullet+}-MV^{\bullet+}\cdot 2X^-$ and $T_8$*$-MV^{2+}\cdot 2X^-$, by which $T_8^{\bullet+}-MV^{\bullet+}$ may gain the triplet character.

The transient absorption spectra of $T_4-MV^{2+}\cdot 2PF_6^-$ observed by the excitation of the $T_4$ moiety in $CH_3CN$ are shown in Figure 7A. The absorption band at 1080 nm was attributed to the radical cation of $T_4$ ($T_4^{\bullet+}$) with $\epsilon_{T_4^{\bullet+}} = 13\,600$ $M^{-1}$ $cm^{-1}$.[7,20a] It has been reported that $T_4^{\bullet+}$ has a sharp absorption at 680 nm with $\epsilon_{T_4^{\bullet+}} = 37\,500$ $M^{-1}$ $cm^{-1}$. Thus, the shoulder at 660 nm in Figure 7A can be attributed to the $T_4^{\bullet+}$ moiety.[7,20a] In the absorption range of 550−620 nm, the absorption band of the $MV^{\bullet+}$ moiety appeared as a shoulder,[26] because this band may be overlapped with the sharp peak at 680 nm of the $T_4^{\bullet+}$ moiety.[7,20a] The relative absorption intensities of the peaks at 1080, 680, and 600 nm (1:2:1) indicate the presence of $T_4^{\bullet+}-MV^{\bullet+}\cdot 2X^-$. This implies that the $^3T_4$* moiety was already

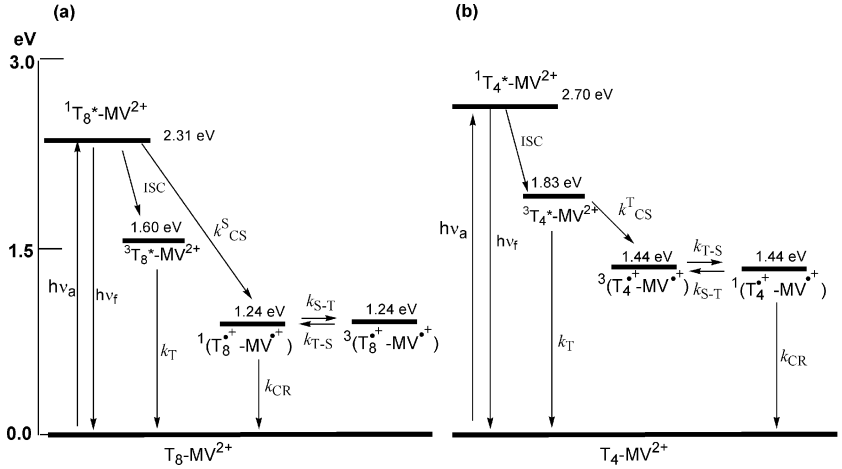


**Figure 8.** Energy diagrams for (a) $T_8-MV^{2+}$ and (b) $T_4-MV^{2+}$ in $CH_3CN$.

decayed at 0.1 $\mu$s. Thus, the charge separation process may take place via the $^3T_4$* moiety, which was supported by the fluorescence lifetime measurement in which fluorescence quenching was not observed for $^1T_4$*$-MV^{2+}$.

The decay time profiles of $T_4^{\bullet+}-MV^{\bullet+}\cdot 2X^-$ are shown in Figure 7B. Because $T_4^{\bullet+}-MV^{\bullet+}\cdot 2X^-$ appeared immediately after the irradiation of the nanosecond laser-light pulse with duration of 6 ns, the rate of generation ($k^T_{CS}$) may be faster than $10^8$ s$^{-1}$. The two-component decay was observed for $T_4^{\bullet+}-MV^{\bullet+}\cdot 2X^-$. From the initial fast decay, which is the main component (75%), the $k_{CR}$ values are estimated to be $4.2-4.8 \times 10^5$ s$^{-1}$ (Table 3). The lifetimes of $T_4^{\bullet+}-MV^{\bullet+}\cdot 2X^-$ were evaluated to be 210−240 ns, which is shorter than those of $T_8^{\bullet+}-VM^{\bullet+}\cdot 2X^-$ (720−980 ns) by a factor of $^1/_3-^1/_5$.

The later, minor slow parts of $T_4^{\bullet+}-MV^{\bullet+}\cdot 2X^-$ in Figure 7B decay in the time region of longer than 10 $\mu$s, which can be attributed to the intermolecular electron transfer.

**$O_2$ Effect on Decay Rates.** Upon addition of $O_2$ into $CH_3CN$ solution, the transient absorption bands of $T_4^{\bullet+}-MV^{\bullet+}$ decayed quickly, as shown in the time profiles in Figure 7B. A similar $O_2$ effect was observed for $T_8^{\bullet+}-MV^{\bullet+}$, in addition to quick decay of the $^3T_n$* moiety (Figure 6). Usually, $T_8^{\bullet+}$and $T_4^{\bullet+}$ do not react with $O_2$, although electron transfer from the $MV^{\bullet+}$ moiety to $O_2$ takes place in a nearly diffusion-controlled rate.[1,30] Therefore, as a reason for the fast decay of $T_n^{\bullet+}-MV^{\bullet+}\cdot 2X^-$ in the presence of $O_2$, we considered that $T_8^{\bullet+}-MV^{\bullet+}\cdot 2X^-$ and $T_4^{\bullet+}-MV^{\bullet+}\cdot 2X^-$ have the triplet spin character, which is easily quenched by a triplet quencher, $O_2$.[20] As for reasons to gain the triplet spin character for the radical ion pairs, one can consider that the precursor of $T_4^{\bullet+}-MV^{\bullet+}\cdot 2X^-$ is $^3T_4$*$-MV^{2+}\cdot 2X^-$. In the case of $T_8^{\bullet+}-MV^{\bullet+}\cdot 2X^-$, the spin character can be borrowed from $^3T_8$*$-MV^{2+}\cdot 2X^-$, which has 0.35-eV higher energy level than that of $T_8^{\bullet+}-MV^{\bullet+}\cdot 2X^-$.

It is possible to consider the sequential intermolecular processes for the decay of $T_n^{\bullet+}-MV^{\bullet+}$ by $O_2$; at first, electron transfer occurs from the $MV^{\bullet+}$ moiety to $O_2$, leaving the $T_n^{\bullet+}$ moiety with the radical anion of $O_2$ ($O_2^{\bullet-}$). Then, it is expected that the decay rates of the $T_n^{\bullet+}$ moiety increase with electron transfer from $O_2^{\bullet-}$. However, such intermolecular processes must be slower than the rate observed in Figure 7b in the presence of $O_2$.[27]

**Energy Diagrams.** The energy diagrams can be drawn from $E_{0-0}$ (T) and $\Delta G_{RIP}$ as shown in Figure 8. The $\Delta G^S_{CS}$ value for $T_8-MV^{2+}\cdot 2X^-$ (−1.05 through −1.10 eV) is less negative than that of $T_4-MV^{2+}\cdot 2X^-$ (−1.34 eV), and charge separation occurs only for $T_8-MV^{2+}\cdot 2X^-$ via $^1T_8$*; thus, these data suggest that the reorganization energy is rather near 1.0 eV.[28] Because the $\Delta G^T_{CS}$ value for $T_4-MV^{2+}\cdot 2X^-$ (−0.38 eV) is almost the same to that for $T_8-MV^{2+}\cdot 2X^-$ (−0.36 through −0.40 eV), the charge separation route is mainly determined by the difference of the $\Delta G^S_{CS}$ values.

Because the $\Delta G_{CR}$ value for $T_8^{\cdot+}-MV^{\cdot+}\cdot 2X^-$ (−1.24 through −1.19 eV) is less negative than that of $T_4^{\cdot+}-MV^{\cdot+}\cdot 2X^-$ (−1.44 eV), slow $k_{CR}$ for $T_8^{\cdot+}-MV^{\cdot+}\cdot 2X^-$ and $T_4^{\cdot+}-MV^{\cdot+}\cdot 2X^-$ cannot be explained by the reorganization energy of ∼1.0 eV. Rather, longer lifetimes of the charge separation state for $T_8^{\cdot+}-MV^{\cdot+}\cdot 2X^-$ than for $T_4^{\cdot+}-MV^{\cdot+}\cdot 2X^-$ can be attributed to the longer $R_{CC}$ value of $T_8-MV^{2+}\cdot 2X^-$ (ca. 22 Å) than that of $T_4-MV^{2+}\cdot 2X^-$ (ca. 11 Å).

## Conclusion

In the present study, the charge separation process for $T_8^{\bullet+}-MV^{\bullet+}\cdot 2X^-$ predominantly occurs via the $^1T_8$* moiety, while the charge separation process for $T_4^{\bullet+}-MV^{\bullet+}\cdot 2X^-$ occurs via the $^3T_4$* moiety. Long $\tau_{RIP}$ values in the region of 210−980 ns were found for $T_8^{\bullet+}-MV^{\bullet+}\cdot 2X^-$ and $T_4^{\bullet+}-MV^{\bullet+}\cdot 2X^-$ in $CH_3CN$, which can be explained by the slow charge recombination between the positively charged species and the triplet character of the radical ion pairs. Longer $\tau_{RIP}$ values for $T_8^{\bullet+}-MV^{\bullet+}\cdot 2X^-$ than those for $T_4^{\bullet+}-MV^{\bullet+}\cdot 2X^-$ were rationalized by the distance between the radical cation centers.

## Experimental Section

**Molecular Orbital Calculations.** Geometry optimization and calculations of molecular orbital coefficients were performed using the semiempirical PM3 method in MOPAC.[23]

**Apparatus.** Reduction potentials ($E_{red}$'s) and oxidation potentials ($E_{ox}$'s) were measured by cyclic voltammetry on a potentiostat (EGG PAR 273 A) in a conventional three-electrode cell equipped with Pt working and counter electrodes with a $Ag/Ag^+$ reference electrode at scan rates of 100 mV s$^{-1}$. In each case, the solution containing 1 mM sample with 0.05 M *n*-$Bu_4NPF_6$ (Fluka purest quality) was deaerated with argon bubbling.

Steady-state fluorescence spectra of the samples were measured on a Shimadzu RF-5300PC spectrofluorophotometer. Fluorescence lifetimes were measured by a single-photon counting method using a streakscope (Hamamatsu Photonics, C4334-01). The samples were excited with the second harmonic generator (410 nm) of a Ti:sapphire laser (Spectra-Physics, Tsunami 3950-L2S, fwhm 1.5 ps) equipped with a pulse selector

**SCHEME 2**

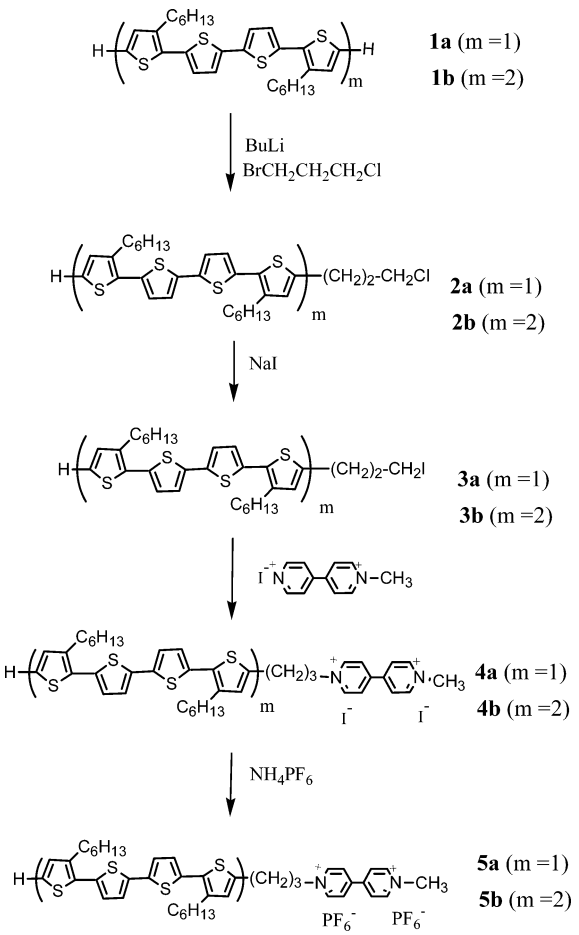


(Spectra-Physics, 3980) and a harmonic generator (Spectra-Physics, GWU-23PS).[29]

Steady-state absorption spectra in the visible and near-IR regions were measured on a Jasco V530 spectrophotometer. Nanosecond transient absorption measurements were carried out using a Nd:YAG laser. For selective excitation of the samples, the output of an optical parametric oscillator (OPO) laser (Continuum Surelite OPO and Surelite II-10) was employed as an excitation source. For short time-scale measurements (<2 $\mu$s), the probe light from a pulsed Xe lamp was detected with a Ge avalanche photodiode equipped with a monochromator after passing through the sample in a quartz cell (1 cm × 1 cm). Long time-scale phenomena (>2 $\mu$s) were observed by using a continuous Xe lamp as a probe light. Sample solutions were deaerated by bubbling Ar gas through the solutions for 15 min. Details of the transient absorption measurements have been described in our previous papers.[29]

**Materials.** Syntheses of $T_4-MV^{2+}\cdot 2X^-$ and $T_8-MV^{2+}\cdot 2X^-$ where $X^- = I^-$ and $PF_6^-$ were performed according to the route as shown in Scheme 2. To explain it briefly, one terminal side of $T_4$ (**1a**) and $T_8$ (**1b**)[22a] was first lithiated with butyllithium and then chloropropylated with 1-bromo-3-chloropropane. After the thus-obtained chloropropyl $T_4$ (**2a)** and $T_8$ (**2b**) were converted to the iodopropyl derivatives **3a** and **3b** by treatment with sodium iodide, the addition of 1-methyl-4,4′-bipyridinyl-1-ium iodide ($MV^+\cdot I^-$) finally yielded $T_4-MV^{2+}\cdot 2I^-$ (**4a)** and $T_8-MV^{2+}\cdot 2I^-$ (**4b)**. Anion exchange with $NH_4PF_6$ also afforded the corresponding $PF_6^-$ salts (**5a** and **5b**). Synthetic details of **4a**, **4b**, **5a**, and **5b** are described in the text to follow, while those of **2a**, **2b**, **2a**, and **3b** are summarized in the Supporting Information.

**General.** All chemicals are of reagent grade. Melting points are uncorrected. $^1$H NMR spectra were measured on a JEOL Lambda 400 spectrometer using deuteriochloroform or deuteriodimethyl sulfoxide as the solvent and tetramethylsilane as the internal standard. MS spectra were recorded on a Shimadzu KOMPACT-MALDI PROBE spectrometer using a dithranol matrix.

**1-[3-(3,3‴-Dihexyl-2,2′;5′,2″;5″,2‴-quaterthiophen-5-yl)-propyl]-1′-methyl-4,4′-bipyridinium iodide (4a).** A mixture of **3a** (3.0 g, 4.5 mmol; see Supporting Information) and 1-methyl-4,4′-bipyridinyl-1-ium iodide[22b] (2.0 g, 6.7 mmol) in 1:1 $CH_3CN-$chloroform (50 mL) was refluxed for 6 days in a nitrogen atmosphere. After evaporation of the solvent, the residual solid was thoroughly washed with hexane and then recrystallized from $CH_3CN$ to give a brown powder (1.7 g, 40%): mp 176−178 °C; $^1$H NMR (400 MHz, DMSO-$d_6$) $\delta$ 0.83−0.85 (m, 6H), 1.25−1.31 (m, 12H), 1.54−1.58 (m, 4H), 2.31 (m, 2H), 2.65 (t, $J$ = 7.6 Hz, 2H), 2.73 (t, $J$ = 8.0 Hz, 2H), 2.88 (t, $J$ = 7.6 Hz, 2H), 4.18 (s, 3H), 4.77 (t, $J$ = 7.6 Hz, 2H), 6.82 (s, 1H), 7.03 (d, $J$ = 3.7 Hz, 1H), 7.04 (d, $J$ = 5.4 Hz, 1H), 7.13 (d, $J$ = 3.9 Hz, 1H), 7.31 (d, $J$ = 3.9 Hz, 1H), 7.32 (d, $J$ = 3.7 Hz, 1H), 7.48 (d, $J$ = 5.4 Hz, 1H), 8.73 (d, $J$ = 6.8 Hz, 2H), 8.77 (d, $J$ = 7.0 Hz, 2H), 9.27 (d, $J$ = 6.8 Hz, 2H), 9.37 (d, $J$ = 6.8 Hz, 2H); MS (MALDI−TOF) $m/z$ 709.4 ($M^+-2I$). Anal. calcd for $C_{42}H_{50}I_2N_2S_4$: C, 52.28; H, 5.22; N, 2.90%. Found: C, 52.25; H, 5.21; N, 2.88%.

**1-[3-(3,3‴,4″,3‴-Tetrahexyl-2,2′;5′,2″;5″,2‴;5″,2‴;5‴,2‴;5‴,2‴;5‴,2‴-octithiophen-5-yl)propyl]-1′-methyl-4,4′-bipyridinium iodide (4b).** This compound was obtained in 20% yield from **3b** (see Supporting Information) in a similar manner as stated already, as a brown powder from $CH_3CN$: mp 2l2−214 °C; $^1$H NMR (400 MHz, DMSO-$d_6$) $\delta$ 0.84−0.85 (m, 12H), 1.28−1.40 (m, 24H), 1.58−1.69 (m, 8H), 2.37 (m, 2H), 2.66−2.74 (m, 8H), 2.89 (t, $J$ = 7.6 Hz, 2H), 4.41 (s, 3H), 4.77 (t, $J$ = 7.6 Hz, 2H), 6.83 (s, 1H), 7.04 (d, $J$ = 5.6 Hz, 1H), 7.05 (d, $J$ = 3.6 Hz, 1H), 7.15 (d, $J$ = 3.9 Hz, 1H), 7.20 (d, $J$ = 3.9 Hz, 1H), 7.21 (d, $J$ = 3.9 Hz, 1H), 7.29 (s, 1H), 7.30 (s, 1H), 7.34 (d, $J$ = 3.9 Hz, 1H), 7.35 (d, $J$ = 3.9 Hz, 1H), 7.37 (d, $J$ = 4.2 Hz, 2H), 7.38 (d, $J$ = 4.0 Hz, 1H), 7.49 (d, $J$ = 5.1 Hz, 1H), 8.73 (d, $J$ = 6.8 Hz, 2H), 8.77 (d, $J$ = 6.8 Hz, 2H), 9.27 (d, $J$ = 6.8 Hz, 2H), 9.37 (d, $J$ = 7.0 Hz, 2H); MS (MALDI−TOF) $m/z$ 1205.9 ($M^+-2I$). Anal. calcd for $C_{70}H_{82}I_2N_2S_8$: C, 57.52; H, 5.65; N, 1.92%. Found: C, 57.46; H, 5.59; N, 1.90%.

**1-[3-(3,3‴-Dihexyl-2,2′;5′,2″;5″,2‴-quaterthiophen-5-yl)-propyl]-1′-methyl-4,4′-bipyridinium hexafluorophosphate (5a).** Compound **4a** (500 mg, 0.52 mmol) was dissolved in 3:1 water−THF (2 mL) and treated with aqueous saturated $NH_4PF_6$ (5 mL). The resulting precipitate was collected and washed with water to give a dark yellow powder (478 mg, 92%): mp 208−211 °C; $^1$H NMR (400 MHz, DMSO-$d_6$) $\delta$ 0.84−0.85 (m, 6H), 1.25−1.31 (m, 12H), 1.54−1.58 (m, 4H), 2.37 (m, 2H), 2.66 (t, $J$ = 8.8 Hz, 2H), 2.73 (t, $J$ = 8.0 Hz, 2H), 2.89 (t, $J$ = 7.6 Hz, 2H), 4.41 (s, 3H), 4.76 (t, $J$ = 7.6 Hz, 2H), 6.82 (s, 1H), 7.03 (d, $J$ = 3.7 Hz, 1H), 7.04 (d, $J$ = 5.1 Hz, 1H), 7.13 (d, $J$ = 3.9 Hz, 1H), 7.31 (d, $J$ = 3.7 Hz, 1H), 7.48 (d, $J$ = 5.4 Hz, 1H), 8.72 (d, $J$ = 7.1 Hz, 2H), 8.75 (d, $J$ = 7.1 Hz, 2H), 9.26 (d, $J$ = 6.8 Hz, 2H), 9.36 (d, $J$ = 6.8 Hz, 2H); MS (MALDI−TOF) $m/z$ 709.4 ($M^+-2PF_6$). Anal. calcd for $C_{42}H_{50}F_{12}N_2P_2S_4$: C, 50.39; H, 5.03; N, 2.80%. Found: C, 50.39; H, 4.96; N, 2.83%.

**1-[3-(3,3‴,4″,3‴-Tetrahexyl-2,2′;5′,2″;5″,2‴;5″,2‴;5‴,2‴;5‴,2‴;5‴,2‴-octithiophen-5-yl)propyl]-1′-methyl-4,4′-bipyridinium hexafluorophosphate (5b).** This compound was obtained in 86% yield from the corresponding iodide (**4b**) in a similar manner as stated already, as a red powder: mp 246−248 °C; $^1$H NMR (400 MHz, DMSO-$d_6$) $\delta$ 0.84−0.85 (m, 12H), 1.28−1.40 (m, 24H), 1.58−1.69 (m, 8H), 2.37 (m, 2H), 2.66−2.74 (m, 8H), 2.89 (t, $J$ = 7.6 Hz, 2H), 4.41 (s, 3H), 4.77 (t, $J$ = 7.6 Hz, 2H), 6.83 (s, 1H), 7.04 (d, $J$ = 5.6 Hz, 1H), 7.05 (d, $J$ = 3.6 Hz, 1H), 7.15 (d, $J$ = 3.9 Hz, 1H), 7.20 (d, $J$ = 3.9 Hz, 1H), 7.21 (d, $J$ = 3.9 Hz, 1H), 7.29 (s, 1H), 7.30 (s, 1H), 7.34 (d, $J$ = 3.9 Hz, 1H), 7.35 (d, $J$ = 3.9 Hz, 1H), 7.37 (d, $J$ = 4.2 Hz, 2H), 7.38 (d, $J$ = 4.0 Hz, 1H), 7.49 (d, $J$ = 5.1 Hz, 1H), 8.73 (d, $J$ = 6.8 Hz, 2H), 8.77 (d, $J$ = 6.8 Hz, 2H), 9.27 (d, $J$ = 6.8 Hz, 2H), 9.37 (d, $J$ = 7.0 Hz, 2H); MS (MALDI−TOF) $m/z$ 1205.7 ($M^+-2PF_6$). Anal. calcd for $C_{70}H_{82}F_{12}N_2P_2S_8$: C, 56.13; H, 5.52; N, 1.87%. Found: C, 56.06; H, 5.56; N, 1.83%.

**Acknowledgment.** This work was supported by a Grant-in-Aid for Scientific Research on Priory Area (417) from the Ministry of Education, Culture, Sports, Science, and Technology (NEXT) of Japanese Government.

**Supporting Information Available:** Synthetic procedures and spectroscopic data to identify the compounds. This material is available free of charge via the Internet at http://pubs.acs.org.

## References and Notes

(1) Calvert, J. M.; Manuccia, T. J.; Nowak, R. J. *J. Electrochem. Soc.* **1986**, *133*, 951.

(2) Monk, P. M. S. *The Viologens;* John Wiley & Sons: Chichester, 1998.

(3) (a) McMahon, R. J.; Force, R. K.; Patterson, H. H.; Wrighton, M. S. *J. Am. Chem. Soc.* **1988**, *110*, 2670. (b) *Photosensitization of Porphryins and Phthalocyanine*s. Okura, I., Ed.; Gordon and Breach Science Publishers: Amsterdam, 2001. (c) Liu, Y.; Nicola, D.; Reiff, O.; Ziessel, R.; Schanzer, K. S. *J. Phys. Chem. A* **2003**, *107*, 3476.

(4) (a) Ebbesen, T. W.; Ferraudi, G. *J. Phys. Chem.* **1993**, *98*, 3717. (b) Ebbesen, T. W.; Manring, L. E.; Peter, K. S. *J. Am. Chem. Soc.* **1984**, *106*, 7400.

(5) (a) Alam, M. M.; Ito, O. *J. Phys. Chem. A* **1999**, *103*, 1306. (b) Konishi, T.; Fujitsuka, M.; Ito, O.; Toba, Y.; Usui, Y. *J. Phys. Chem. A* **1999**, *103*, 9938. (c) Islam, S. D.-M.; Konishi, T.; Fujitsuka, M.; Ito, O.; Nakamura, Y.; Usui, Y. *Photochem. Photobiol.* **2000**, *71*, 675. (d) Konishi, T.; Fujitsuka, M.; Ito, O.; Toba, Y.; Usui, Y. *Bull. Chem. Soc. Jpn.* **2001**, *74*, 39.

(6) (a) Evans, C.; Weire, D.; Scaiano, J. C.; MacEachern, A.; Arnason, J. T.; Morand, P.; Hollebone, B.; Leitch, L. C.; Philogene, B. J. R. *Photochem. Photobiol.* **1986**, *44*, 441. (b) Scaiano, J. C.; Evans, C.; Arnason, J. T. *J. Photochem. Photobiol., B* **1989**, *3*, 411. (c) Evans, C.; Scaiano, J. C. *J. Am. Chem. Soc.* **1990**, *112*, 2694. (d) Boch, R.; Mohtat, B.; Lear, Y.; Arnason, J. T.; Durst, T.; Scaiano, J. C. *Photochem. Photobiol.* **1996**, *64*, 92. (e) Boch, R.; Mehat, B.; Connolly, T.; Durst, T.; Arnason, J. T.; Redmond, R. W.; Scaiano, J. C. *J. Photochem. Photobiol.* **1996**, *93*, 39.

(7) (a) Bennati, M.; Grupp, A.; Baeuerie, P.; Mehring, M. *Mol. Cryst. Liq. Cryst. Sci, Technol., Sect A* **1994**, *256*, 751. (b) Matsumoto, K.; Fujitsuka, M.; Sato, T.; Onodera, S.; Ito, O. *J. Phys. Chem. B* **2000**, *104*, 11632. (c) Cravino, A.; Zerza, G.; Neugebauer, H.; Maggini, M.; Bucella, S.; Menna, E.; Svensson, M.; Andersson, M. R.; Brabec, C.; Sacriciftci, N. S. *J. Phys. Chem. B* **2002**, *106*, 76.

(8) *Electron-Transfer Process in Imaging*; Eaton, D. F., Mattay, J., Eds.; Springer-Verlag: Berlin, 1990; p 199.

(9) (a) Wasielewski, M. R. *Chem. Rev.* **1992**, *92*, 435. (b) Lewis, F. D.; Letsinger, R. L.; Wasielewski, M. R. *Acc. Chem. Res.* **2001**, *34*, 159.

(10) *Fundamentals of Photoinduced Electron Transfer*; Kavarnos, G. J., Ed.; VCH: New York, 1993; p 103.

(11) Gust, D.; Moore, T. A. Moore, A. L. *Photochemical and Photoelectrochemical Conversion and Storage of Solar Energy*; Tian, Z. W., Cao, Y., Eds.; International Academic Publishers: Beijing, 1993.

(12) (a) Maruyama, K.; Osuka, A.; Mataga, N. *Pure Appl. Chem.* **1994**, *66*, 867. (b) Osuka, A.; Mataga, N.; Okada, T. *Pure Appl. Chem.* **1997**, *69*, 797.

(13) (a) Wasielewski, M. R.; Niemczyk, M. P.; Svec, W. A.; Pewitt, E. B. *J. Am. Chem. Soc.* **1985**, *107*, 1080. (b) Asahi, T.; Ohkohchi, M.; Matsusaka, R.; Mataga, N.; Zhang, R. P.; Osuka, A.; Maruyama, K. *J. Am. Chem. Soc.* **1993**, *115*, 5665. (c) Macpherson, A. N.; Liddeel, P. A.; Lin, S.; Noss, L.; Seely, G. R.; DeGraziano, J. M.; Moore, A. L.; Moore, T. A.; Gust, D. *J. Am. Chem. Soc.* **1995**, *117*, 7202.

(14) (a) Gust, D.; Moore, T. A.; Moore, A.; Macpherson, A. N.; Lopez, A.; DeGraziano, J. K.; Gouni, L.; Bittersmann, E.; Seely, G. R.; Gao, F.; Nieman, R. A.; Ma, X. C.; Demache, L. J.; Hung, S.-C.; Luttrull, D. K.; Lee, S.-J.; Kerrigan, P. K. *J. Am. Chem. Soc.* **1993**, *115*, 11141. (b) Kashiwagi, Y.; Ohkubo, K.; MacDonald, J. A,; Blake, I. M.; Crossley, M. J.; Araki, Y.; Ito, O.; Imahori, H.; Fukuzumi, S. *Org. Lett.* **2003**, *5*, 2719. (c) Ohkubo, K.; Kotani, H.; Shao, J.; Ou, Z.; Kadeshi, K.; Li, G.; Pandey, R. K.; Fujitsuka, M.; Ito, O.; Imahori, H.; Fukuzumi, S. *Angew. Chem., Int. Ed.* **2004**, *43*, 853.

(15) (a) Marcus, R. A. *J. Chem. Phys.* **1956**, *24*, 966. (b) Marcus, R. A. *J. Chem. Phys.* **1965**, *43*, 679. (c) Marcus, R. A.; Sutin, N. *Biochim. Biophys. Acta* **1985**, *811*, 265.

(16) (a) Imahori, H.; Hagiwara, K.; Akiyama, T.; Aoki, M.; Taniguchi, S.; Okada, T.; Shirakawa, M.; Sakata, Y. *Chem. Phys. Lett.* **1996**, *263*, 545. (b) Imahori, H.; Tamaki, K.; Guldi, D. M.; Luo, C.; Fujitsuka, M.; Ito, O.; Sakata, Y.; Fukuzumi, S. *J. Am. Chem. Soc.* **2001**, *123*, 2607.

(17) (a) Komamine, S.; Fujitsuka, M.; Ito, O.; Moriwaki, K.; Miyata, T.; Ohno, T. *J. Phys. Chem. A* **2000**, *104*, 11497. (b) Yamazaki, M.; Araki, Y.; Fujitsuka, M.; Ito, O. *J. Phys. Chem. A* **2001**, *105*, 8615. (c) Imahori, H.; EL-Khouly, M. E.; Fujitsuka, M.; Ito, O.; Sakata, Y.; Fukuzumi, S. *J. Phys. Chem. A* **2001**, *105*, 325.

(18) (a) Becker, R. S.; de Melo, J. S.; Maçanita, A. L.; Elisei, F. *Pure Appl. Chem.* **1995**, *67*, 9. (b) Becker, R. S.; de Melo, J. S.; Maçanita, A. L.; Elisei, F. *J. Phys. Chem.* **1996**, *100*, 18683. (c) de Melo, J. S.; Silva, L. M.; Arnaut, L. G.; Becker, R. S. *J. Chem. Phys.* **1999**, *111*, 5427.

(19) (a) Walters, K. A.; Trouillet, L.; Guillerez, S.; Schanze, K. S. *Inorg. Chem.* **2000**, *39*, 5496. (b) Shen, Y.; Walters, K. A.; Abboud, K.; Schanze, K. S. *Inorg. Chim. Acta* **2000**, *414*, 300. (c) Walters, K. A.; Premvardhan, L. L.; Liy, Y.; Peteann, L. A.; Schanze, K. S. *Chem. Phys. Lett.* **2001**, *339*, 255. (d) Liu, Y.; Nicoals, A. D.; Reiff, O.; Ziessel, R.; Schanze, K. S. *J. Phys. Chem. A* **2003**, *107*, 3476.

(20) (a) Fujitsuka, M.; Ito, O.; Yamashiro, T.; Aso, Y.; Otsubo, T. *J. Phys. Chem. A* **2000**, *104*, 4876. (b) Fujitsuka, M.; Matsumoto, K.; Ito, O.; Yamashiro, T.; Aso, Y.; Otsubo, T. *Res. Chem. Intermed.* **2001**, *27*, 73. (c) Fujitsuka, M.; Masuhara, A.; Ito, O.; Kasai, H.; Oikawa, H.; Nakanishi, H.; Yamashiro, T.; Aso, Y.; Otsubo, T. *J. Phys. Chem. B* **2001**, *105*, 9930.

(21) (a) van Hal, P. A.; Knol, J.; Langeveld-Voss, B. M. W.; Meskers, S. C. J.; Hummelen, J. C.; Janssen, R. A. J. *J. Phys. Chem. A* **2000**, *104*, 5974. (b) van Hal, P. A.; Beckers, E. H. A.; Meskers, S. C. J.; Janssen, R. A. J.; Jousselme, B.; Blanchard, P.; Roncali, J. *Chem.—Eur. J.* **2002**, *8*, 5415. (c) Beckers, E. H. A.; van Hal, P. A.; Dhanabalan, A.; Meskers, S. C. J.; Knol, J.; Hummelen, J. C.; Janssen, R. A. J. *J. Phys. Chem. A* **2003**, *107*, 6218.

(22) (a) Yamashiro, T.; Aso, Y.; Otsubo, T.; Tang, H.; Harima, T.; Yamashita, K. *Chem. Lett.* **1999**, 443. (b) Pileni, M.-P.; Braun, A. M.; Grätzel, M. *Photochem. Photobiol.* **1980**, *31*, 423.

(23) Steweart, J. J. P. *J. Comput. Chem.* **1989**, *10*, 209.

(24) (a) Rehm, D.; Weller, A. *Isr. J. Chem.* **1970**, 8, 259. (b) Weller, A. *Z. Phys. Chem. Neue Folge* **1982**, *133*, 93.

(25) Arbogast, J. W.; Foote, C. S.; Kao, M. *J. Am. Chem. Soc.* **1992**, *114*, 2277.

(26) (a) Harriman, A.; Mills, A. *J. Chem. Soc., Faraday Trans. 2* **1981**, *77*, 2111. (b) Watanabe, T.; Honda, K. *J. Phys. Chem.* **1982**, *86*, 2617. (c) Kim, Y.-S.; McNiven, S.; Ikebukuro, K.; Karube, I. *Photochem. Photobiol.* **1997**, *66*, 180.

(27) Consumption of the $T_n^{\bullet+}$ moiety in $T_n^{\bullet+}-MV^{\bullet+}$ can be observed in the presence of $O_2$, if hole transfer to the $MV^{2+}$ moiety occurs after electron transfer from the $MV^{\bullet+}$ moiety to $O_2$ in nearly diffusion-controlled rate; however, such hole-transfer process from the $T_n^{\bullet+}$ moiety to the $MV^{2+}$ moiety is thermodynamically difficult to occur.

(28) (a) Harrison, R. J.; Pearce, B.; Beddard, G. S.; Cowan, J. A.; Sanders, J. K. *Chem. Phys.* **1987**, *116*, 429. (b) DeGrazíano, J. M.; Liddel, P. A.; Leggett, L.; Moore, A. L.; Moore, T. A.; Gust, D. *J. Phys. Chem.* **1994**, *98*, 1758. (c) Tsue, H.; Imahori, H.; Kaneda, T.; Tanaka, Y.; Okada, T.; Tamaki, K.; Sakata, Y. *J. Am. Chem. Soc.* **2000**, *122*, 2279.

(29) (a) Choi, M. S.; Aida, T.; Luo, H.; Araki, Y.; Ito, O. *Angew. Chem., Int. Ed.* **2003**, *42*, 4060. (b) Luo, H.; Fujitsuka, M.; Araki, Y.; Ito, O.; Padmawar, P.; Chiang, L. Y. *J. Phys. Chem. B* **2003**, *107*, 9312. (c) Guo, X.; Gan, Z.; Luo, H.; Araki, Y.; Zhang, D.; Zhu, D.; Ito, O. *J. Phys. Chem. A* **2003**, *107*, 9747. (d) Yamanaka, K.; Fujitsuka, M.; Araki, Y.; Ito, O.; Aoshima, T.; Fukushima, T.; Miyashi, T. *J. Phys. Chem. A* **2004**, *108*, 250.